Extreme ultraviolet interferometric measurements of diffraction-limited optics

Kenneth A. Goldberg[a] and Patrick Naulleau
Center for X-Ray Optics, Lawrence Berkeley National Laboratory, Berkeley, California 94720

Jeffrey Bokor
Center for X-Ray Optics, Lawrence Berkeley National Laboratory, Berkeley, California 94720
and EECS Department, University of California, Berkeley, California 94720

(Received 2 June 1999; accepted 9 September 1999)

At-wavelength interferometric measurements of recently fabricated extreme ultraviolet (EUV) microstepper projection optics have revealed the highest performance for prototype EUV lithographic systems observed to date. The phase-shifting point diffraction interferometer is used to measure and align these two-mirror, multilayer-coated Schwarzschild optical systems designed with a numerical aperture of 0.088 and operating at 13.4 nm wavelength. Root-mean-square wave front error magnitudes as small as 0.60 nm have been achieved, actually exceeding the design tolerance set for these objectives. © *1999 American Vacuum Society.* [S0734-211X(99)06106-5]

I. INTRODUCTION

Extreme ultraviolet (EUV) lithography is being developed as a candidate technology to follow deep ultraviolet lithography for feature sizes below 100 nm. This development has been greatly facilitated by the use of small-field microstepper projection optics which have been used for a variety of demonstration experiments.[1] Recently, several new microstepper objectives have been fabricated with the goal of achieving considerable improvement in lithographic resolution as well as reduced flare. These two-mirror, multilayer-coated Schwarzschild objectives operate near normal incidence with 13 nm wavelength light, a numerical aperture (NA) as high as 0.088, and 10× demagnification. They are identical in optical design to the previous generation of EUV optics used in the development of EUV lithographic technologies; yet the new optical substrates are fabricated to much stricter figure and finish tolerances.

We report at-wavelength interferometric measurements on these systems which reveal the highest optical performance for prototype EUV lithographic systems achieved to date. The enhanced imaging performance from these new optics[1] is due both to improvements in the figure and to a reduction in the midspatial-frequency roughness that contributes to flare. The root-mean-square (rms) wave front error magnitudes in three separate systems are 0.63 nm (0.047 waves at 13.4 nm wavelength), 0.60 nm (0.045 waves), and 0.99 nm (0.074 waves), respectively, within 0.088 NA. The flare from two of these optics has been measured at below 4.5%.

Achieving diffraction-limited performance from EUV optical systems has required the development of interferometry with subangstrom accuracy. The Virtual National Laboratory (VNL), in cooperation with the EUV Limited Liability Company (EUV LLC), is conducting parallel development of EUV wave front testing with a phase-shifting point diffraction interferometer (PS/PDI)[2] and visible-light phase-shifting diffraction interferometry (PSDI)[3,4] for the measurement of lithographic-quality, multiple-element, aspherical optical systems. These two diffraction-based interferometers have demonstrated the required accuracy necessary for the development of EUV lithographic optical systems.

Visible-light PSDI measurement is now used during the fabrication of individual spherical and aspherical components, before and after multilayer coating. It is also used during the alignment of multielement optical systems. At present, EUV PS/PDI testing is reserved for the qualification and possible final alignment of assembled optical systems.

Visible-light has clear advantages in optical shop testing, where it can be used to measure single uncoated elements. Yet the EUV wave front is determined both by the geometric figure of the mirror surfaces and by the properties of the multilayer coatings, which are deposited across mirror areas covering many square centimeters. It is for this reason that at-wavelength EUV testing is the most direct probe of the sensitive resonance properties of reflective multilayer coatings. Coating thickness gradients, designed to achieve optimal reflectivity in the presence of a range of incidence angles, and surface contamination can cause differences between visible-light and EUV wave front measurements. Recent cross-comparison experiments have shown favorable agreement between EUV and visible-light wave front measurements in four separate Schwarzschild objectives;[5] and ongoing EUV imaging experiments performed at Sandia National Laboratory have demonstrated the power of EUV interferometry in successfully predicting imaging performance.[1,6]

We present EUV wave front measurements performed on three recently fabricated Schwarzschild objectives, called cameras A, B1, and B2. These optics share the same optical design and a common mechanical housing configuration. At-wavelength fine alignment was performed on cameras A and B2, while camera B1 measurements are presented as it was delivered for EUV measurement.

The two reflective elements of camera A were fabricated to meet the same figure specifications set forth for the mirrors in the new projection optics box (PO box), the

[a]Electronic mail: KAGoldberg@lbl.gov

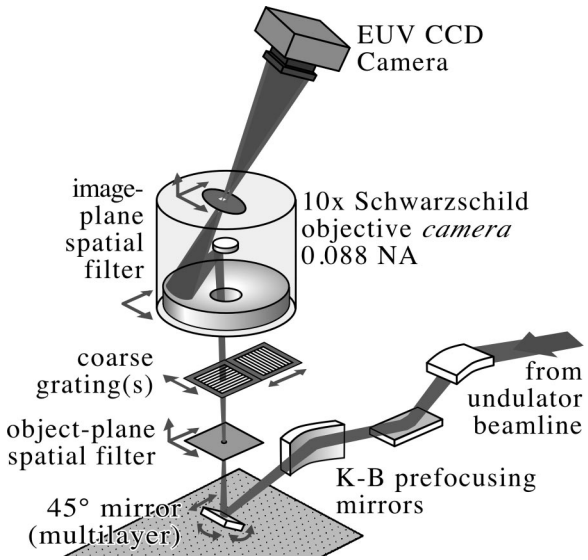

FIG. 1. Schematic of the EUV PS/PDI configured to measure a 10× Schwarzschild objective *camera* in a vertical orientation. The interferometer is contained in a vacuum chamber. Arrows indicate degrees of freedom for the optical elements.

4× EUV imaging system being developed by the VNL.[7] The elements of cameras B1 and B2 have even higher quality, having been fabricated to meet both the figure and the finish specifications of the PO box. A comparison of EUV and visible-light interferometric wave front measurements performed using cameras A and B1 has been presented in a previous publication.[4] Following initial interferometric measurement, the mirror elements of camera A were removed from their mechanical housing. They were subsequently reassembled into a new housing, and only new, post-reassembly measurements are presented here.

II. EUV INTERFEROMETRY

The EUV PS/PDI, first proposed by Medecki *et al.*,[8–10] is a common-path interferometer that relies on pinhole diffraction to produce spherical reference waves. Using coherent illumination from an undulator beamline at the Advanced Light Source synchrotron radiation facility,[11] the EUV PS/PDI has become one of the most accurate system-level measurement tools of its kind. Its reference wave front accuracy has been demonstrated to be as high as 0.04 nm rms in a NA of 0.082,[12] well beyond the present requirements for EUV optical system metrology.

Figure 1 shows a schematic representation of the EUV PS/PDI. Details of its construction and use have been extensively described.[12–14] The PS/PDI uses a pair of pinholes placed at conjugate object and image points to produce spherical reference wave fronts. The object pinhole spatially filters the incident light to produce a spherical illuminating beam. Via transmission, the illuminating beam acquires the aberrations of the test optic and becomes the test beam. The test beam comes to focus in the image plane and then propagates to reach the detector, which is placed significantly beyond the image plane.

To create the reference beam, a small-angle beamsplitter is placed before the test optic; a relatively coarse transmission grating makes a convenient beamsplitter for this application. The grating produces multiple copies of the test beam, focused in the image plane with a small lateral separation. A patterned opaque membrane in the image plane is used to selectively transmit and block the focused beams. One of these beams is transmitted through a *window* (large compared to the focused beam's diameter) and becomes the test beam. A second beam is brought to focus on a nearby pinhole spatial filter called the reference pinhole. The reference pinhole is fabricated smaller than the diffraction-limited resolution of the test optical system to produce a filtered spherical reference wave front. The test and reference beams propagate to a mixing plane, where their interference is recorded by an EUV CCD detector.

To be suitable for EUV operation and resistant to carbon contamination, the EUV PS/PDI operates *in vacuo* at a base pressure of 10^{-6} Torr, backfilled with oxygen to a partial pressure of 4×10^{-6} Torr.

III. ASSEMBLY AND ALIGNMENT

The optical design of the two-mirror EUV Schwarzschild imaging systems under investigation uses an off-axis circular subaperture of the full annular pupil. Selected from several possible combinations, individual *primary* and *secondary* mirrors are paired to form the highest quality wave fronts possible. The pairing is based on visible-light interferometric measurements of individual mirror elements and on detailed performance simulations that include the rotational *clocking* of the mirrors' azimuthal orientations.[15]

Alignment of the assembled Schwarzschild objectives is first performed using a visible-light PSDI developed and operating at Lawrence Livermore National Laboratory. The optics are then transported to Lawrence Berkeley National Laboratory for at-wavelength characterization and, in some cases, additional alignment using the EUV PS/PDI operating at the Advanced Light Source. EUV imaging experiments performed at Sandia National Laboratory provide confirmation of the near-diffraction-limited performance predicted by the wave front measurements.

Wave front aberrations vary, depending on the object and conjugate image point locations. Therefore, careful selection of the conjugate points is an essential element of measurement accuracy. To this end, a pair of functionally equivalent alignment fixtures has been fabricated to guarantee longitudinal and lateral agreement between the conjugate points used in both the visible-light and EUV interferometers and in imaging experiments.

Final mirror-alignment adjustments are made via two screws that control the tilt of the convex primary mirror. An aperture stop placed in close proximity to the surface of the primary defines a stationary beam *footprint* on that mirror's surface. Tilt adjustments to the primary do, however, affect the location of the beam on the concave secondary mirror, which in turn affects the wave front—primarily in terms of

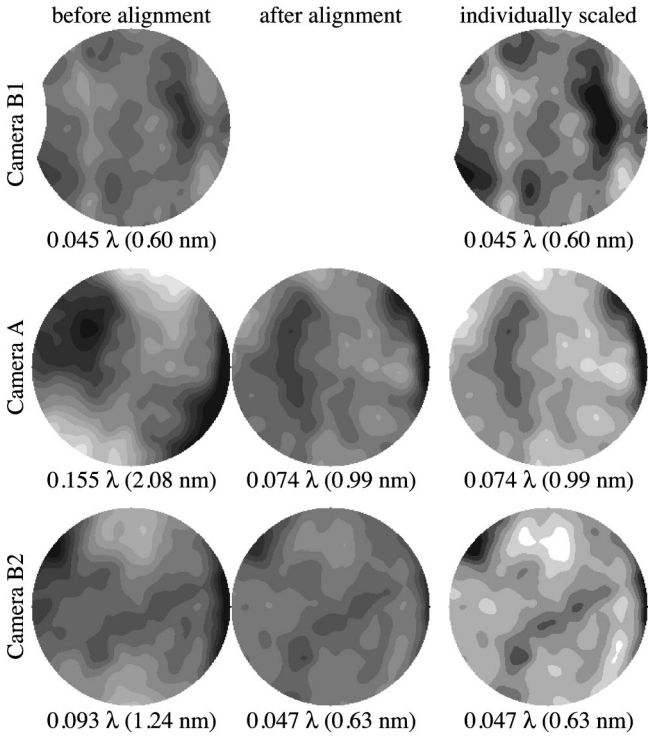

FIG. 2. Cameras B1, A, and B2 wave fronts measured before and after alignment. Left and center columns are shown using the same grayscale: contours are shown with three gray levels per nanometer. Individually scaled wave fronts are shown in the right column with two gray levels per nanometer rms wave front error magnitudes are shown below each wavefront, based on 37-term Zernike fitting; however, the wave fronts shown contain more of the available spatial frequency content. The wavelength of measurement λ is 13.4 nm.

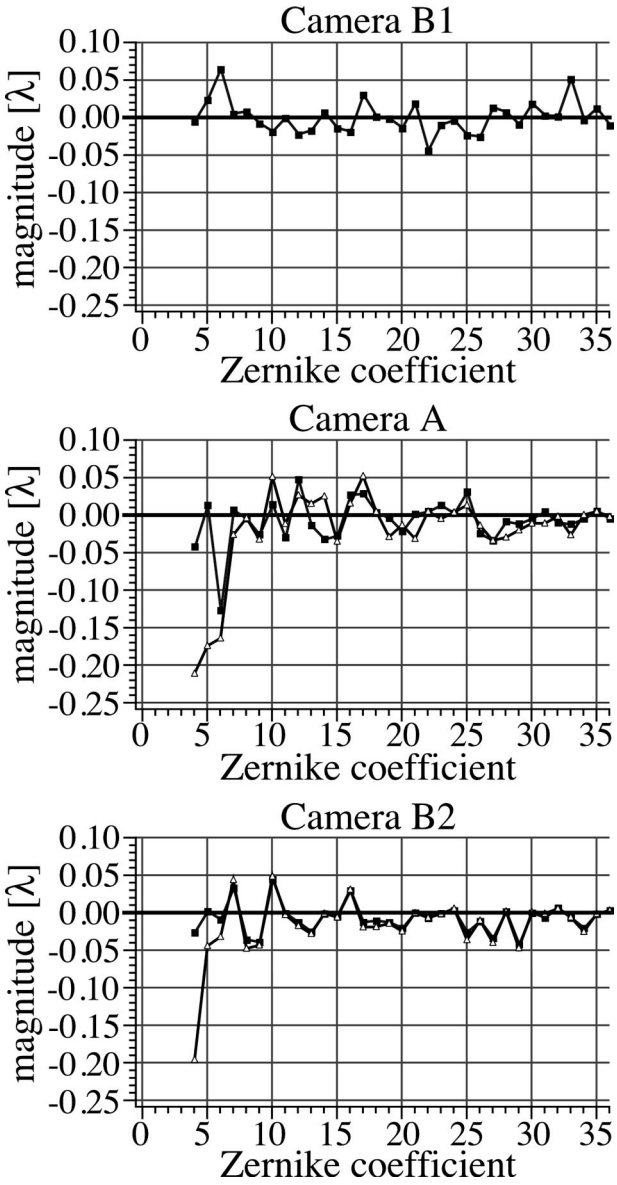

FIG. 3. Zernike polynomial coefficients describing the wave fronts from cameras B1, A, and B2. For cameras A and B2, open triangles denote coefficients before alignment, and solid squares after alignment.

astigmatism. The wave front error minimization is achieved by systematically steering the beam until astigmatism is minimized.

Within the Zernike description, a wavefront, Φ, may be approximated by a Zernike series, $\Phi = \Sigma a_j Z_j$. The convention employed here has the individual orthogonal Zernike polynomials bounded in the range $[-1, 1]$ on a unit circle domain. Counting from an index ''0'' as the *piston* term, the two astigmatism coefficients are a_4 and a_5 representing 0° and 45° astigmatism, respectively. For a unit magnitude Zernike coefficient, the corresponding peak-to-valley wave front error contribution is two, and the rms contribution is typically about 0.4, although rms magnitudes add in quadrature.

During alignment, a relatively small degree of unpredictability is introduced by irregularities in the mirror surfaces, particularly the secondary mirror. As the beam footprint on the secondary mirror moves, features on the surface move into and out of the illuminated region.

IV. WAVE FRONT MEASUREMENTS

In chronological order, EUV interferometry was performed on cameras B1, A, and then B2. EUV-based alignment was performed only on cameras A and B2. Figure 2 contains wave front measurements of the three optics before and (in the cases of cameras A and B2) after EUV alignment. In the left and central columns of Fig. 2 the five wave fronts are represented using the same grayscale; in the right-most column, the three wavefronts are shown using individual grayscale representations. In all cases, the rms wave front error magnitudes shown are based on fits to the first-37 Zernike polynomials.[16,17] The Zernike polynomial coefficients for each of the five wavefronts are plotted in Fig. 3. The measurement-dependent *piston*, *tilt*, and *defocus* coefficients (a_0 through a_3) are excluded. Measurement uncertainties for the Zernike coefficients are below 6×10^{-3} waves (0.07 nm), based on the wave front fitting uncertainty ($<5\times10^{-4}$ waves), the measurement-to-measurement repeatability ($<2\times10^{-3}$ waves), and the measured accuracy of

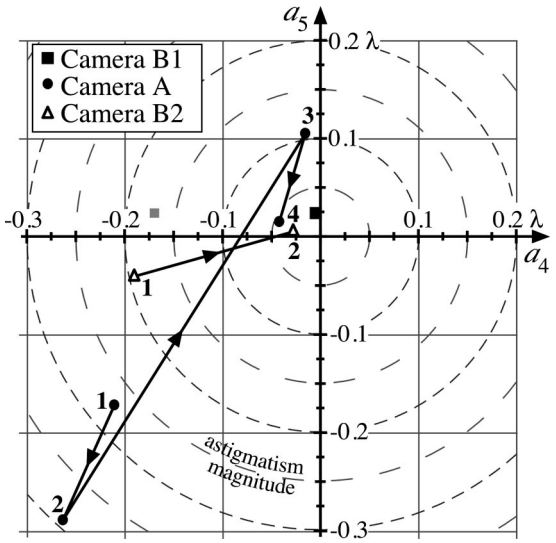

FIG. 4. Wave front astigmatism coefficients a_4 and a_5 from the Zernike polynomial fit are used to guide the alignment. Plotted are four measurements from the alignment of camera A, two measurements from camera B2, and one measurement point from camera B1 (dark solid square). Measurement sequence is indicated by numbers adjacent to the points. Based on camera B1's measured wave front and the known displacement from the design conjugate position, the gray solid square predicts the wave front at the design conjugates.

the EUV PS/PDI (6×10^{-3} waves rms in the full wave front, using similarly sized reference pinholes as were used to perform these measurements).

Measurement of camera B1 was performed before the aforementioned alignment fixture had been developed for the EUV interferometer. In this case, with no mechanical reference to serve as a guide, positioning of the conjugate object and image points was based on the location of the wave front-error minimum. Using the alignment fixture, we have subsequently observed that our measurements had been conducted from an object field point displaced longitudinally by 2.5 mm from the nominal position. The consequences of the displacement, studied using a computer model of the Schwarzschild objective, reveal that measurements made at the nominal position would show an additional astigmatism contribution of approximately 0.32 waves, peak-to-valley, or 0.16 waves in the Zernike coefficient of 0° astigmatism.

The individual steps of the alignment procedure are well illustrated by their effect on the astigmatism coefficients in the Zernike polynomial description. These coefficients guide the adjustments iteratively until an acceptable alignment has been achieved. Figure 4 contains a two-axis plot of the Zernike coefficients a_4 and a_5 for all three cameras.

Camera A was the first one aligned at-wavelength. Figure 4 shows that although the first adjustment was accidentally made with the wrong polarity, subsequent iterations reduced the astigmatism coefficients to less than 0.05 waves (0.67 nm). The alignment sensitivity matrix calculated during the alignment of camera A was applied to the alignment of camera B2, enabling the astigmatism to be removed with only one adjustment. This is also shown in Fig. 4.

The single measurement of camera B1 is shown in Fig. 4 as a black solid square close to the origin. As stated earlier, this measurement was made at a longitudinally displaced field point. The predicted astigmatism coefficients for this optic, if it were measured at the nominal field point, are shown as a gray solid square near the x axis.

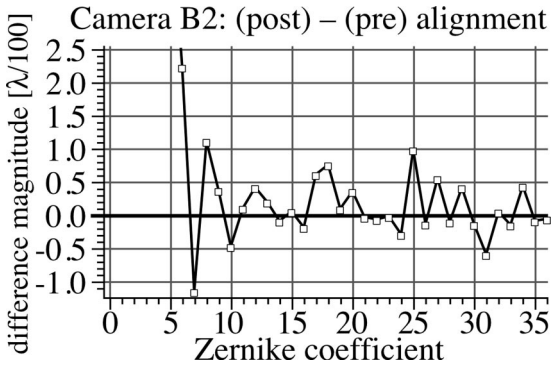

FIG. 5. Excepting astigmatism and coma (coefficients 4 through 7) which are used in the alignment, the small differences between the wave front coefficients from two alignment steps shows the high level of repeatability in the EUV PS/PDI.

One important aspect of these EUV optical system alignment exercises is the robustness and repeatability they demonstrate, for both the interferometer and the optical housing. Between each iteration, the vacuum chamber must be vented, the optic is lifted entirely out of the chamber, a 4 lb image-plane stage assembly that rests on the wafer side of the optic is removed, clamp screws that control the primary mirror's gimbals mount are loosened, and the appropriate alignment adjustments are made. The system is then reassembled, the vacuum chamber lid, to which the charge coupled device detector is attached, is replaced, and the system is pumped down for 2–3 h. Excluding the astigmatism and coma coefficients (a_4 through a_7), which are affected by the alignment procedure, the measurement-to-measurement repeatability of the higher-order Zernike coefficients is excellent. In Fig. 5, the coefficient *differences* between the initial and final iterations of camera B2 are shown. Most coefficients are well within λ/200, nearly all are within λ/100.

V. CONCLUSION

At-wavelength alignment of an EUV Schwarzschild objective has produced the smallest wave front error observed to date in an EUV optical system—0.045 waves rms (0.60 nm, or ~λ/72) within 0.088 NA. The alignment procedure is robust and predictable. Improvements of the system wave front over previous alignments may push the system closer toward diffraction-limited EUV imaging performance.

ACKNOWLEDGMENTS

The authors wish to thank Paul Denham and Phil Batson of LBNL, Ken Stewart of SNL for essential engineering contributions, and Henry Chapman of LLNL for assistance with alignment strategies. This research has been supported by the EUV LLC, the Semiconductor Research Corporation, the

DARPA Advanced Lithography Program, and by the Office of Basic Energy Sciences of the U.S. Department of Energy.

[1]J. E. M. Goldsmith *et al.*, Proc. SPIE **3676**, 264 (1999).
[2]K. A. Goldberg, P. Naulleau, S. Lee, C. Bresloff, D. Attwood, and J. Bokor, J. Vac. Sci. Technol. B **16**, 3435 (1998).
[3]G. E. Sommargren, in *OSA Trends in Optics and Photonics*, Extreme Ultraviolet Lithography, Vol. 4, edited by G. D. Kubiak and D. R. Kania (Optical Society of America, Washington, DC, 1996), pp. 108–112.
[4]G. E. Sommargren, Laser Focus World **32**, 61 (1996).
[5]K. A. Goldberg *et al.*, Proc. SPIE **3676**, 635 (1999).
[6]E. Tejnil, K. A. Goldberg, S. H. Lee, H. Medecki, P. J. Batson, P. E. Denham, A. A. MacDowell, and J. Bokor, J. Vac. Sci. Technol. B **15**, 2455 (1997).
[7]D. W. Sweeney, R. Hudyma, H. N. Chapman, and D. Shafer, Proc. SPIE **3331**, 2 (1998).
[8]H. Medecki, E. Tejnil, K. A. Goldberg, and J. Bokor, Opt. Lett. **21**, 1526 (1996).
[9]H. Medecki, US Patent No. 5,835,217 (Nov. 1998).
[10]E. Tejnil, K. A. Goldberg, H. Medecki, R. Beguiristain, J. Bokor, and D. T. Attwood, OSA TOPS Volume on Extreme Ultraviolet Interferometry (1996).
[11]D. T. Attwood *et al.*, IEEE J. Quantum Electron. **35**, 709 (1999).
[12]P. Naulleau, K. A. Goldberg, S. Lee, C. Chang, C. Bresloff, P. Batson, D. Attwood, and J. Bokor, Proc. SPIE **3331**, 114 (1998).
[13]K. A. Goldberg, E. Tejnil, S. H. Lee, H. Medecki, D. T. Attwood, K. H. Jackson, and J. Bokor, Proc. SPIE **3048**, 264 (1997).
[14]K. A. Goldberg, Ph.D. dissertation, Department of Physics, University of California, Berkeley, 1997.
[15]A. K. Ray-Chaudhuri (personal communication).
[16]A. B. Bathia and E. Wolf, Proc. Phys. Soc. London, Sect. B **65**, 909 (1952).
[17]D. J. Fischer, J. T. O'Bryan, R. Lopez, and H. P. Stahl, Appl. Opt. **32**, 4738 (1993).